Climate-Adaptive Photothermal Superhydrophobic CA/PU Membrane for Oil-Water Separation

Supporting Information

Enyu Wei ,†[a] Ye Zhang,†[a] Linfei Pan,[a] Lili Li [a, *]

[a] *Key Laboratory of Automobile Materials, Ministry of Education, and College of Materials Science and Engineering, Jilin University, Changchun 130022, China.*

† These two authors are joint first authors.

** Corresponding author.*

E-mail: lilyllee@jlu.edu.cn (Lili Li)

Supplementary Notes

Note S1. Preparation of CA/PU$_x$ composite membrane

Cellulose acetate (CA) was dissolved in tetrahydrofuran (THF) to prepare solution A with different concentrations. Subsequently, 1.2 g of polyurethane (PU) was introduced into 10 mL of dimethylformamide (DMF), and the mixture was heated to 100 °C until the PU was completely dissolved, thereby preparing solution B. After that, solutions A and B were combined in an equal-volume ratio to yield the final spinning solution. The relevant experimental details were summarized in Table S2.

Electrospinning was performed under the following conditions: a voltage of 16 kV was applied, the distance between the needle and the collector was set at 15 cm, and the solution was fed at a rate of 1 mL h^{-1} using a syringe pump. The ambient temperature and relative humidity were maintained at 25 °C and 50% relative humidity (RH), respectively. The prepared composite membranes were designated as CA/PU$_1$, CA/PU$_2$, CA/PU$_3$ and CA/PU$_4$.

Note. S2. Characterizations

The morphological characteristics of the sample were observed using field emission scanning electron microscope (FE-SEM; JSM-6700F, JEOL, Japan). The energy dispersive spectroscopy (EDS, JSM-7900, JEOL, Japan) was employed to identify the element distribution. The composition and crystal structure of the samples were precisely analyzed via X-ray diffraction (XRD) technique, employing the Siemens D5000 X-ray diffractometer (Germany) for the measurements. The structural characteristics of the samples were characterized by Fourier transform infrared spectroscopy utilizing the FTIR-4100 instrument (JASCO, Japan). The surface chemical components of samples were examined by X-ray photoelectron spectroscopy (XPS; ESCALAB220i-XL, VG Scientific, UK). The laser scanning confocal microscope (LSCM 3EXT, OLYMPUS, Japan) was utilized to examine the surface's roughness. The water contact angle (WCA) of the samples was measured using a drop shape analyzer (DSA100, KRÜSS Scientific, Germany). Dynamic light scattering (using a Zetasizer Nano ZS, UK) was utilized to examine the particle dimensions of the

water-in-oil emulsion. The photocatalytic degradation experiments were conducted using a Xenon light source (PLS-SXE300+, PerfectLight, China). A universal testing apparatus (WSK-5KN, Changchun Intelligent Instrument and Equipment Co., Ltd., China) was utilized to evaluate the mechanical properties. Under normal environmental conditions, each membrane was loaded at a constant rate of 5 mm/min.

Note S3 The cyclic de-icing test of CA/PU_3-P membrane

The CA/PU_3-P membrane was placed on a semiconductor cooling stage and carry out the following steps sequentially: (1) A 100-μm water droplet was added to the membrane; (2) The experimental temperature was adjusted to -10 °C until the droplet was completely frozen; (3) The membrane was placed under simulated sunlight until the water droplet was completely melted. Repeat the above experiment for 5 cycles. Record the freezing and melting times during each cycle respectively.

Supplementary Figures

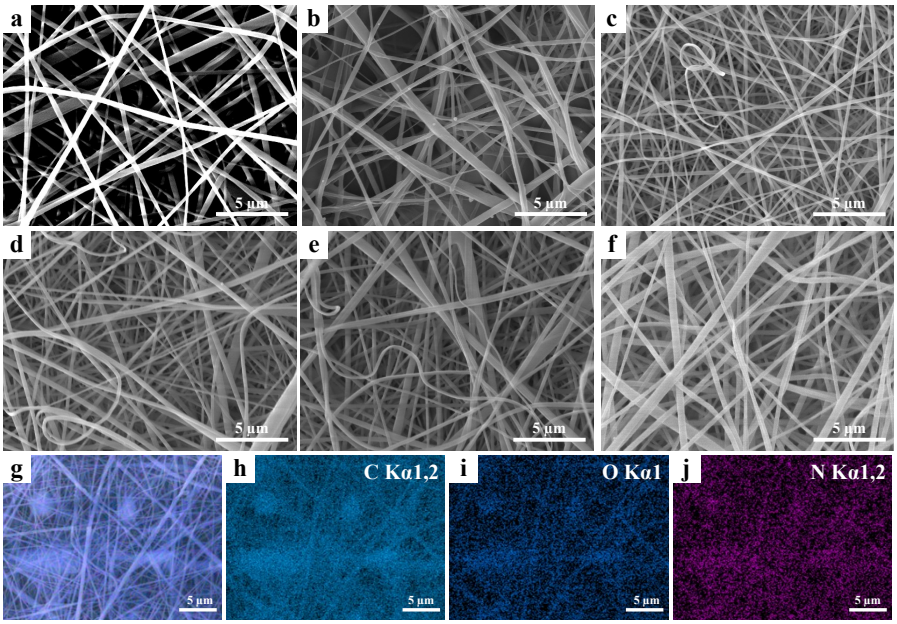

Fig. S1. The morphology of (a) CA, (b) PU, (c) CA/PU_1, (d) CA/PU_2, (e) CA/PU_3 , (f) CA/PU_4. EDS results of CA/PU_3 membrane: (g) SEM image for EDS, mapping images with (h) C (azure), (i) O (blue) and (j) N (pink).

The morphologies of the CA , CA/PU_x and PU membranes were presented in Fig. S1. Fig. S1a showed the microscopic morphology of the CA nanofiber membrane, which was characterized by smooth and continuous fibers. In Fig. S1b, an adhesion phenomenon was observed between the nanofibers of the PU membrane, which might be related to the high boiling point of the DMF solvent[1]. The high-boiling-point solvent evaporated very slowly, resulting in adhesion at the fiber contact points[2]. The fiber structures of CA/PU_x membranes were extremely similar to that of CA and PU (Fig. S1c-f). In Fig. S1g-j,the EDS characterization of CA/PU_3 indicated that the elements C, O, and N a uniformly distribution across the membrane surface.

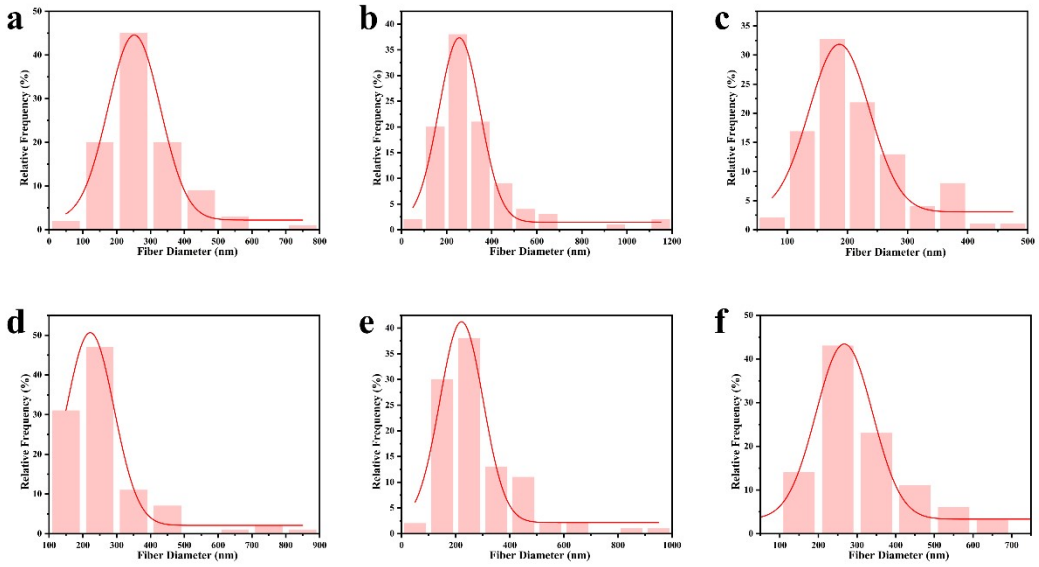

Fig. S2. Diameter distribution diagram of (a) CA, (b)PU, (c) CA/PU_1, (d) CA/PU_2, (e) CA/PU_3, and (f) CA/PU_4 membranes.

The diameters of the CA, PU, CA/PU_1, CA/PU_2, CA/PU_3, and CA/PU_4 fibrous membranes were respectively 251.83 ± 7.01 nm, 256.50 ± 6.15 nm, 186.68 ± 6.84, 221.76 ± 5.07 nm,221.74 ± 9.67 nm, and 267.10 ± 9.90 nm (Fig. S2).

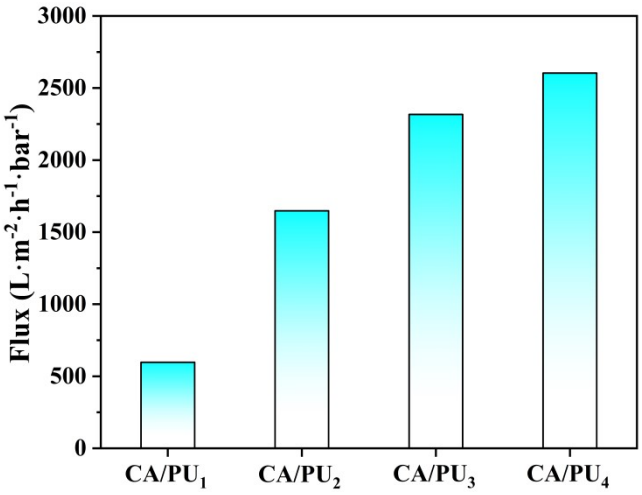

Fig. S3. The permeation flux of n-hexane across the CA/PU_x membranes.

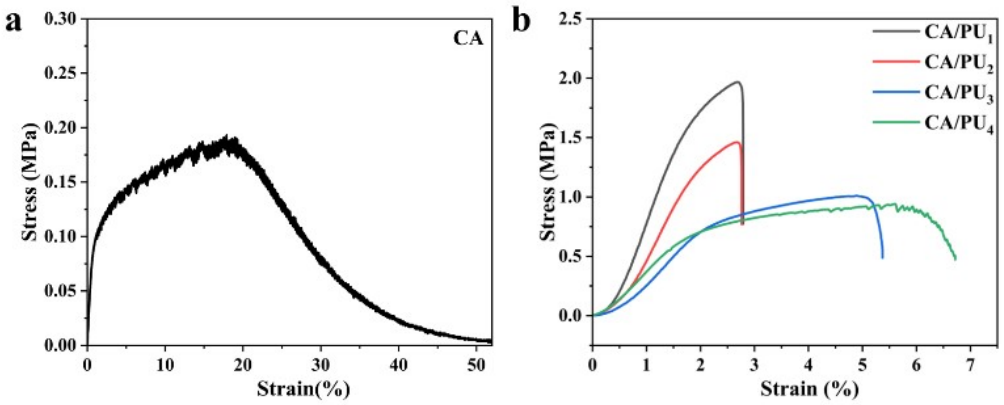

Fig. S4. Tensile tests of (a) CA and (b) CA/PU_x membranes.

As the CA content gradually increased, the membrane flux exhibited a corresponding gradual rise. Among the CA/PU_1, CA/PU_2, CA/PU_3, and CA/PU_4 membranes, their respective fluxes for n-hexane were 597.14, 1648.09, 2316.88 and 2603.50 $L{\cdot}m^{-2}{\cdot}h^{-1}$ (Fig. S1). For the CA/PU_x membranes, with the increasing PU content in the solution, the tensile strength of the membrane exhibited a progressive enhancement, rising from an initial value of 0.94 MPa to a final value of 2.70 MPa (Fig. S4b). The elongation at break increased from 2.7% to 5.9%. After a comprehensive analysis of the mechanical property data of these membranes, the CA/PU_3 membrane was ultimately chosen as the optimal sample.

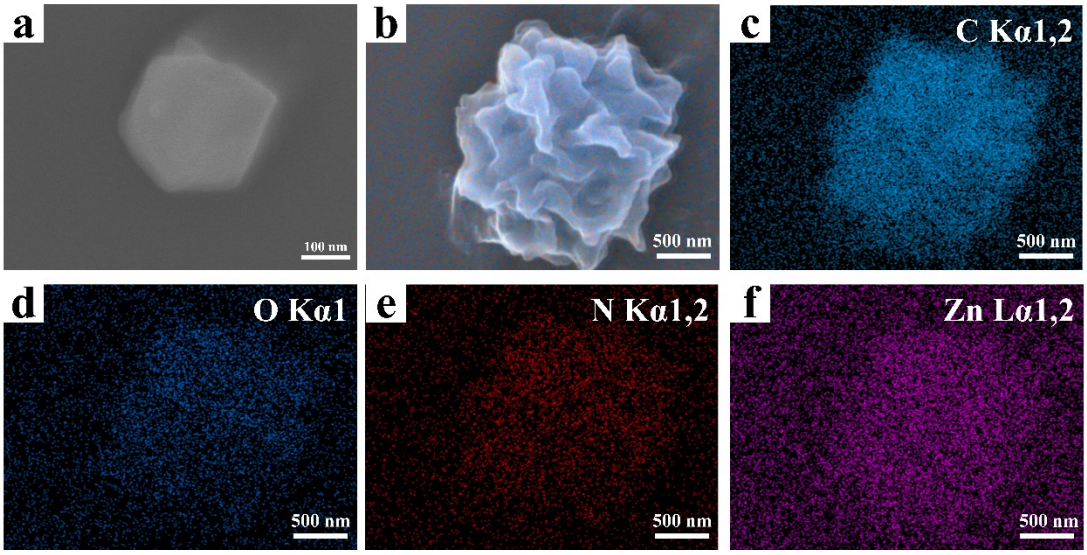

Fig. S5. (a) SEM of ZIF-8. (b) SEM image for EDS of ZIF-8-M, mapping images with (c) C (azure), (d) O (blue), (e) N (red) and (f)Zn (pink).

Fig. S5a showed unmodified ZIF-8 particle, which exhibited an octahedral structure as reported in the literature[3]. Hydrophobic modification ZIF-8 was achieved using oleic acid, an eco–friendly amphiphilic molecule consisting of a hydrophobic long-carbon chain and a hydrophilic carboxyl group at one end. The surface of micron-sized particles exhibited a wrinkled structure. In Fig. S5c-f, the EDS characterization of the ZIF-8-M particle indicated a uniform distribution of the elements C, O, and N across the particle surface. Additionally, a small amount of Zn element was presented on the particle surface, with an atomic percentage of 1 at%.

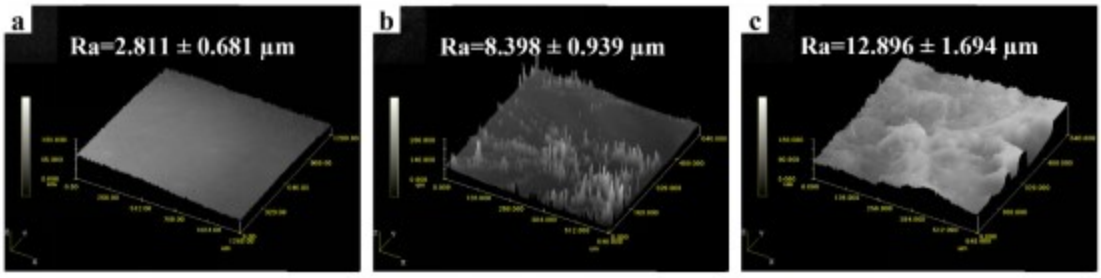

Fig. S6. Roughness images of (a) CA/PU_3, (b) CA/PU_3-P, and (c) CA/PU_3-PZ membranes.

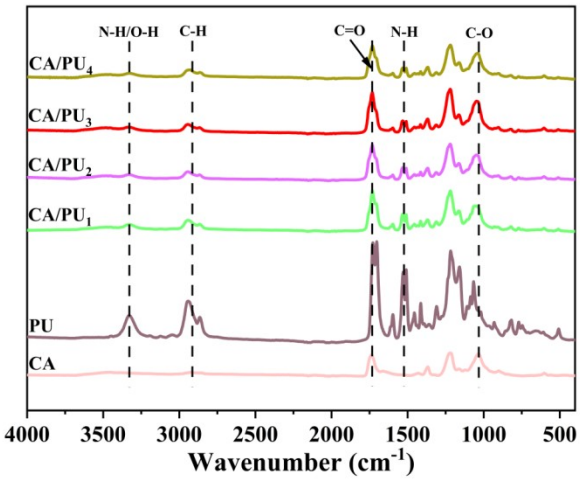

Fig. S7. FTIR spectrum of CA,PU and CA/PU_x membranes.

The FTIR analysis identified absorption peaks at 2918 cm^{-1} (methylene/methine C–H asymmetric stretching vibration), 2850 cm^{-1} (methylene/methine C–H stretching vibration) and 1718 cm^{-1} (C=O stretching vibration) as common functional group signatures in both CA and PU[2]. For CA, the peaks at 3488 cm^{-1} and 1034 cm^{-1} were associated with the O–H stretching and C–O stretching[4]. For PU, the peaks at 3329 cm^{-1} (N-H stretching vibration), 1597 cm^{-1} (aromatic C=C stretching vibration), and

1527 cm^{-1} (N-H bending vibrations) were observed[5].The intensity of N–H stretching and bending vibrations decreased with the increase of CA content, which might result from the formation of hydrogen bonds between the hydroxyl groups of CA and the amino groups of PU.

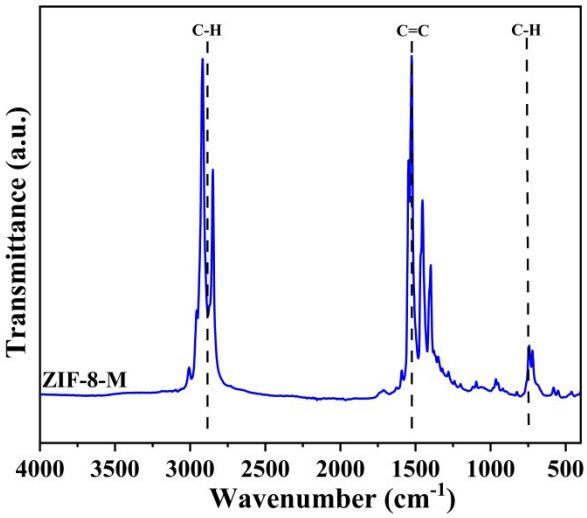

Fig. S8. FTIR spectrum of ZIF-8-M particles.

In FTIR spectra of ZIF-8-M, the peaks observed at 2918 cm^{-1} and 2848 cm^{-1} were associated with the methylene/methine C–H asymmetric stretching vibration and the methylene/methine C–H stretching vibration, respectively[6]. The peak observed at 1527 cm^{-1} corresponded to the stretching vibration of the C=C bond. These findings demonstrated the successful loading of oleic acid molecules and the successful synthesis of ZIF-8-M particles. The characteristic peak observed at 736 cm^{-1} was attributable to the out-of-plane bending vibration of C-H bonds within the ZIF-8-M framework (Fig. S8).

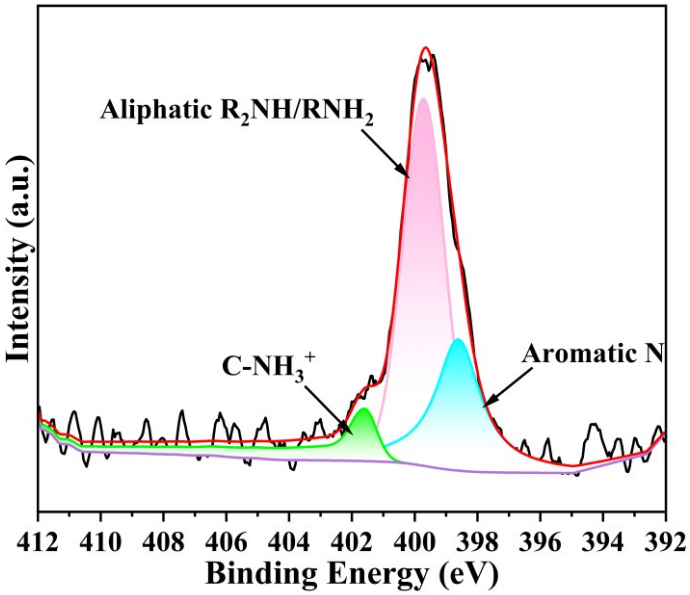

Fig. S9. High-resolution N 1s spectrum of CA/PU_3-P membrane.

As illustrated in Fig. S9, in the high-resolution N 1s spectrum of CA/PU_3–P membrane, the characteristic peaks at 401.6 eV, 399.7 eV, and 398.6 eV were assigned to $C\text{-}NH_3^+$,aliphatic R_2NH/RNH_2 and aromatic N[7].

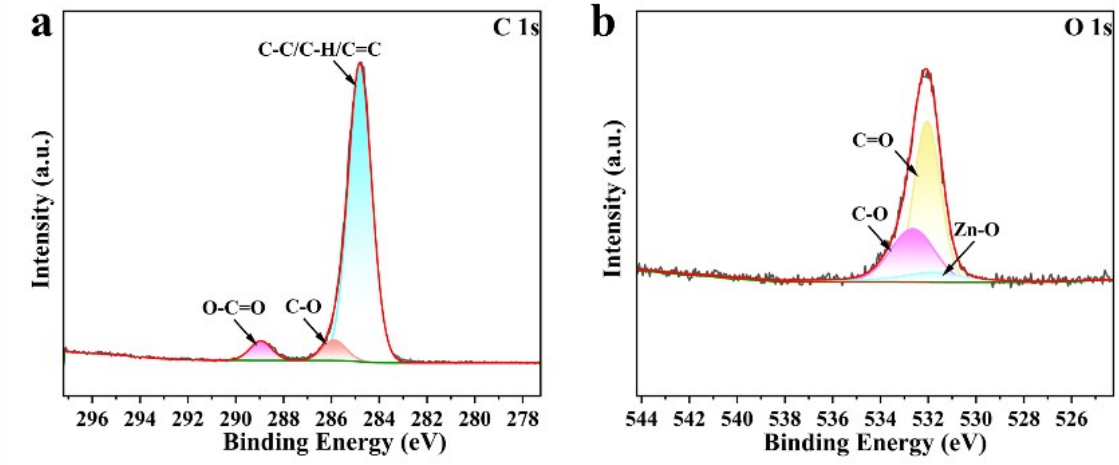

Fig. S10. High-resolution (a) C 1 s and (b) O 1 s spectrum of ZIF-8-M particles.

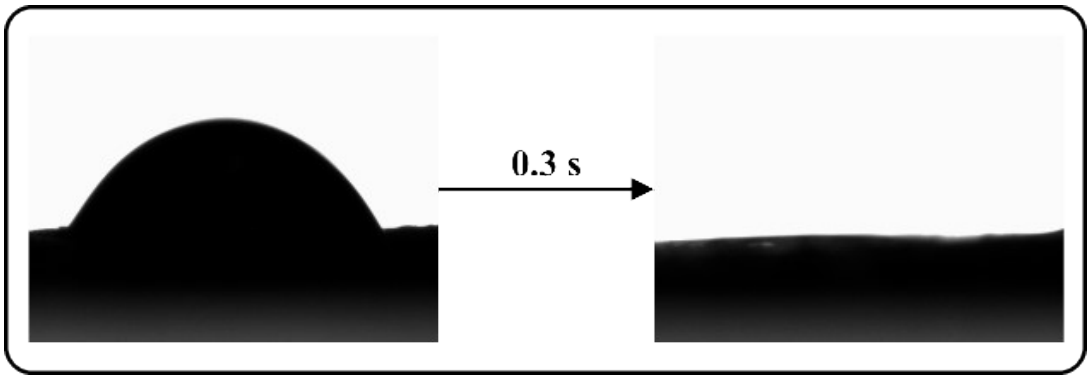

Fig. S11. The temporal evolution of the WCA for CA/PU_3-P.

Fig. S12. Oil-water separation device.

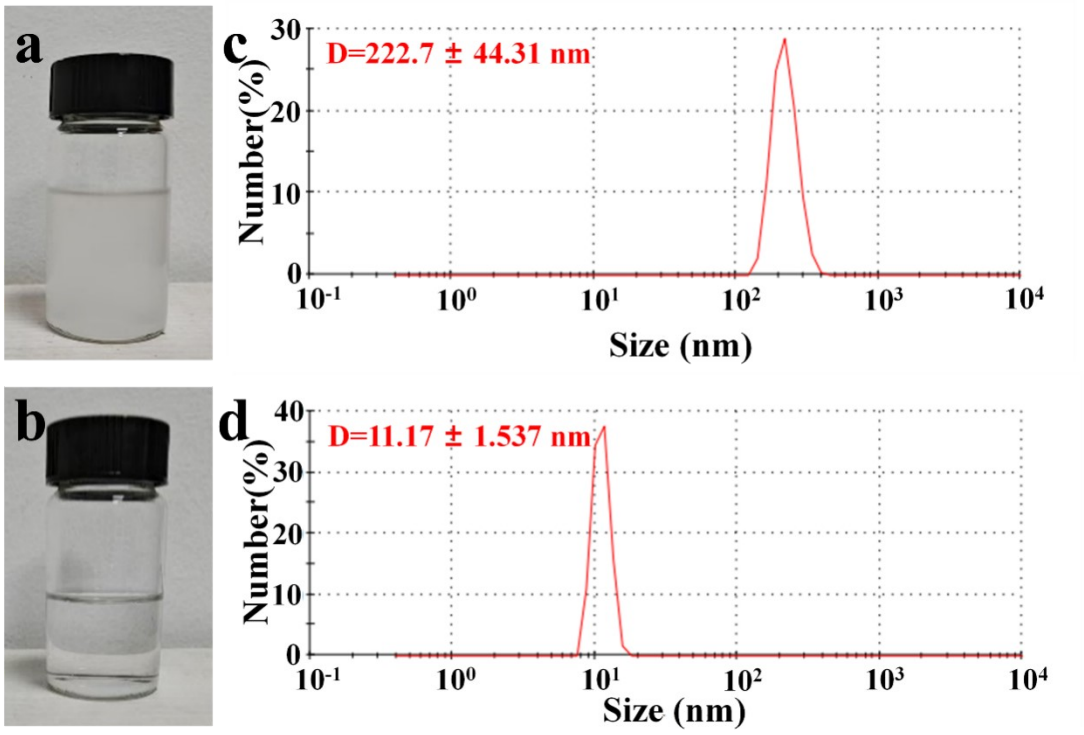

Fig. S13. (a,b) Images and (c,d) particle size distributions of water-in-n-hexane emulsions before

and after separation;

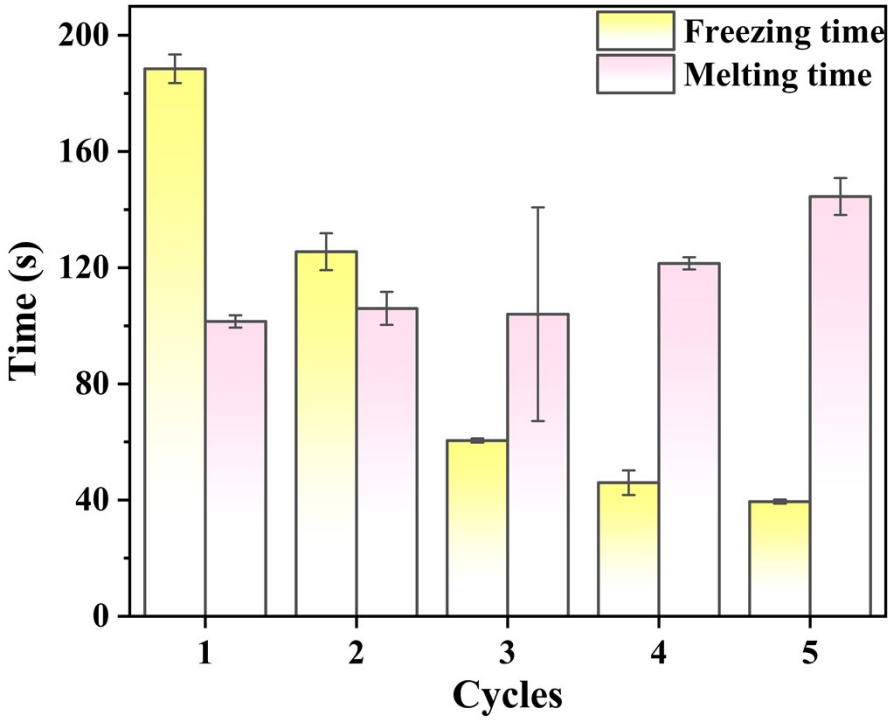

Fig. S14. The freezing time and melting time during the cyclic de-icing test of CA/PU_3-P membrane.

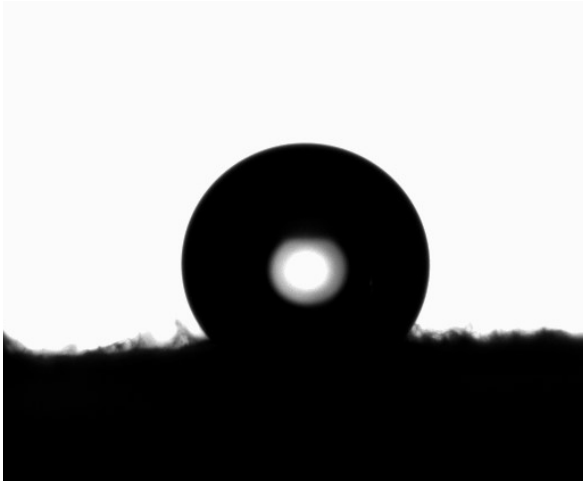

Fig. S15. The WCA of the CA/PU_3-PZ membrane after mechanical de-icing.

Supplementary Tables

Table S1

Comparison of Performance with Other Articles

Flux (L m^{-2} h^{-1})	Separation efficiency (s)	Photothermal temperature (°C)	Temperature (°C)	Photothermal de-icing time (s)	Droplet freezing time (s)	Article
			-5		660	
2.12×10^5	98.5	65.2	-15	135	300	[8]
			-25		180	
-	-	67.4	-10	-	578	[9]
3.67×10^5	99.3	62.8	-	440	-	[10]
-	-	76.6	-15	450	385	[11]
-	-	99	-10	180	960	[12]
-	-	133.8	-15	-	170	[13]
-	-	83.1	-10	156	802	[14]
1584.39	99.6	47.3	-10	355	981	This Article

Table S2

The composition of the precursor solution.

Sample	Solution concentration (wt%)		Dosage ratio
	CA	PU	
CA/PU_1	10	12	1:1
CA/PU_2	12	12	1:1
CA/PU_3	14	12	1:1
CA/PU_4	16	12	1:1

References

1 Tang C, Chen P, Liu H. Cocontinuous cellulose acetate/polyurethane composite nanofiber fabricated through electrospinning[J]. *Polymer Engineering & Science*, 2008, **48(7)**: 1296–1303.

2 Zhang Y, Yang M, Zhou Y, Yao A, Han Y, Shi Y, Cheng F, Zhou M, Zhu P, Tan L. Transition sandwich Janus membrane of cellulose acetate and polyurethane nanofibers for oil–water separation[J]. *Cellulose*, 2022, **29(3)**: 1841–1853.

3 Yang W, Kong Y, Yin H, Cao M. Study on the adsorption performance of ZIF-8 on heavy metal ions in water and the recycling of waste ZIF-8 in cement[J]. *Journal of Solid State Chemistry*, 2023, **326**: 124217.

4 Chen W, Ma H, Xing B. Electrospinning of multifunctional cellulose acetate membrane and its adsorption properties for ionic dyes[J]. *Int J Biol Macromol*, 2020, **158**: 1342–1351.

5 Riaz T, Ahmad A, Saleemi S, Adrees M, Jamshed F, Hai A M, Jamil T. Synthesis and characterization of polyurethane-cellulose acetate blend membrane for chromium (VI) removal[J]. *Carbohydr Polym*, 2016, **153**: 582–591.

6 Yamawaki H, Fujihisa H. Infrared spectra of the β and γ phases of oleic acid under high pressure[J]. *Spectrochimica Acta Part A: Molecular and Biomolecular Spectroscopy*, 2022, **265**: 120290.

7 Yang X, Duan L, Ran X. Effect of polydopamine coating on improving photostability of polyphenylene sulfide fiber[J]. *Polym Bull*, 2017, **74(3)**: 641–656.

8 Qiao L, Zhou Z, Wang M, He Z. Lignin Microsphere/TiO2 Composite-Based Melamine Sponge with Superhydrophobic and Photothermal Properties for Oil/Water Separation and Anti-Icing[J]. *Langmuir*, 2025, **41(21)**: 13233–13248.

9 Wang L, Hu J, Zhou X, Liu M, Wu Y, Zheng H. Modification-free bionic superhydrophobic laser-induced graphene (LIG) wearable strain sensor with superior anti-icing performance[J]. *Chem Eng J*, 2025, **508**: 161140.

10 Wang M, Qiao L, Ma S, He Z. Facile Preparation of Photothermal Superhydrophobic Melamine Sponge Decorated with MXene and Lignin Particles for Efficient Oil/Water Separation, Fast Crude Oil Recovery, and Active Deicing[J]. *Langmuir*, 2024, **40(11)**: 5978–5991.

11 Ma T, Wei J, Sun W, Zhang S, Wang D, Yang X, Zhou Z, Tong W, Wang J. Durable Photothermal Superhydrophobic Coatings with Amorphous-Polymer Composite Structure Enhance Anti-Icing and Environment-Resistant Properties[J]. *Langmuir*, 2025, **41(43)**: 29051–29063.

12 Xiao X, Yao F, Huang M, Wei J, Wang J. Electrothermal-Assisted Photothermal Lubrication Surfaces for Continuous Anti-Icing/Deicing in Multiple Low-Temperature Environments[J]. *Langmuir*, 2024, **40(32)**: 17151–17159.

13 Yang T, Lu Q, Ren F, Xin S, Zhang H, Qiao H, Wang Z, Liu L. A Fluorine-Free Superhydrophobic Micro–Nano Structured SiO2/TiN Coating for Anti-icing and Photothermal Deicing[J]. *ACS Applied Nano Materials*, 2024, **7(12)**: 14737–14747.

14 Liu S, Zhu Z, Zheng Q, Wang K, Zhou F, Yang Q, Wang X, Ye L, Chen Y, Liu H, Li H. Waxberry-liked micro-nanostructured, superhydrophobic surfaces with enhanced photothermal de-icing and passive anti-icing properties[J]. *Chem Eng J*, 2025, **503**: 158358.